RESEARCH ARTICLE

Sphingosine Kinase Regulates Microtubule Dynamics and Organelle Positioning Necessary for Proper G_1/S Cell Cycle Transition in *Trypanosoma brucei*

Deborah A. Pasternack,[a,b,d] Aabha I. Sharma,[a,b,d] Cheryl L. Olson,[a,b,d] Conrad L. Epting,[a,c] David M. Engman[a,b,d]

Department of Pathology,[a] Department of Microbiology-Immunology,[b] Department of Pediatrics,[c] and Feinberg Cardiovascular Research Institute,[d] Northwestern University, Chicago, Illinois, USA

D.A.P. and A.I.S. contributed equally to this work.

ABSTRACT **Sphingolipids are important constituents of cell membranes and also serve as mediators of cell signaling and cell recognition. Sphingolipid metabolites such as sphingosine-1-phosphate and ceramide regulate signaling cascades involved in cell proliferation and differentiation, autophagy, inflammation, and apoptosis. Little is known about how sphingolipids and their metabolites function in single-celled eukaryotes. In the present study, we investigated the role of sphingosine kinase (SPHK) in the biology of the protozoan parasite *Trypanosoma brucei*, the agent of African sleeping sickness. *T. brucei* SPHK (TbSPHK) is constitutively but differentially expressed during the life cycle of *T. brucei*. Depletion of TbSPHK in procyclic-form *T. brucei* causes impaired growth and attenuation in the G_1/S phase of the cell cycle. TbSPHK-depleted cells also develop organelle positioning defects and an accumulation of tyrosinated α-tubulin at the elongated posterior end of the cell, known as the "nozzle" phenotype, caused by other molecular perturbations in this organism. Our studies indicate that TbSPHK is involved in G_1-to-S cell cycle progression, organelle positioning, and maintenance of cell morphology. Cytotoxicity assays using TbSPHK inhibitors revealed a favorable therapeutic index between *T. brucei* and human cells, suggesting TbSPHK to be a novel drug target.**

IMPORTANCE ***Trypanosoma brucei* is a single-celled parasite that is transmitted between humans and other animals by the tsetse fly. *T. brucei* is endemic in sub-Saharan Africa, where over 70 million people and countless livestock are at risk of developing *T. brucei* infection, called African sleeping sickness, resulting in economic losses of ~$35 million from the loss of cattle alone. New drugs for this infection are sorely needed and scientists are trying to identify essential enzymes in the parasite that can be targets for new therapies. One possible enzyme target is sphingosine kinase, an enzyme involved in the synthesis of lipids important for cell surface integrity and regulation of cell functions. In this study, we found that sphingosine kinase is essential for normal growth and structure of the parasite, raising the possibility that it could be a good target for new chemotherapy for sleeping sickness.**

Received 28 August 2015 **Accepted** 1 September 2015 **Published** 6 October 2015

Citation Pasternack DA, Sharma AI, Olson CL, Epting CL, Engman DM. 2015. Sphingosine kinase regulates microtubule dynamics and organelle positioning necessary for proper G_1/S cell cycle transition in *Trypanosoma brucei*. mBio 6(5):e01291-15. doi:10.1128/mBio.01291-15.

Editor Louis M. Weiss, Albert Einstein College of Medicine

Address correspondence to Conrad L. Epting, c-epting@northwestern.edu, or David M. Engman, d-engman@northwestern.edu.

This article is a direct contribution from a Fellow of the American Academy of Microbiology.

Trypanosomatids are parasitic protozoa that cause African sleeping sickness, Chagas disease, and leishmaniases. These trypanosome infections collectively threaten half a billion people worldwide (1). *Trypanosoma brucei*, the causative agent of African sleeping sickness, is transmitted to the bloodstream of a mammalian host by an infected tsetse fly. The African sleeping sickness is endemic to sub-Saharan Africa, where ~70 million people and countless livestock live at risk of contracting sleeping sickness (2), and ~$35 million of economic loss can be attributed to *T. brucei* infection of cattle (3). The signs and symptoms of sleeping sickness are often nonspecific or recognized later in infection, access to health care is poor, and therapeutic regimens are long and toxic. Further, drug treatment has led to the emergence of drug-resistant parasite strains (2). Elucidating complex metabolic pathways and enzymes that are key to essential cellular processes may accelerate the development of new and more effective trypanocidal therapies.

Trypanosomes possess a typical eukaryotic cell cycle, comprised of G_1, S, G_2, and M phases, which are regulated by Cdc2-related kinases (CRKs) and their partner cyclins. The G_1/S phase of the cell cycle is regulated by CRK1-cyclin E1 and CRK2-cyclin E1 (4–6), the latter of which plays a distinct role in posterior-end cell morphogenesis (4, 6). The G_2/M-phase transition is regulated by CRK3-cyclin B2 (4, 5), and yet the mitosis-to-cytokinesis checkpoint is absent (7). In mammalian cells, growth factor stimulation through the mitogen-activated protein kinase (MAPK) pathway promotes the G_1/S-phase transition in a CDK2-cyclin E-dependent manner (8). However, canonical growth factor re-

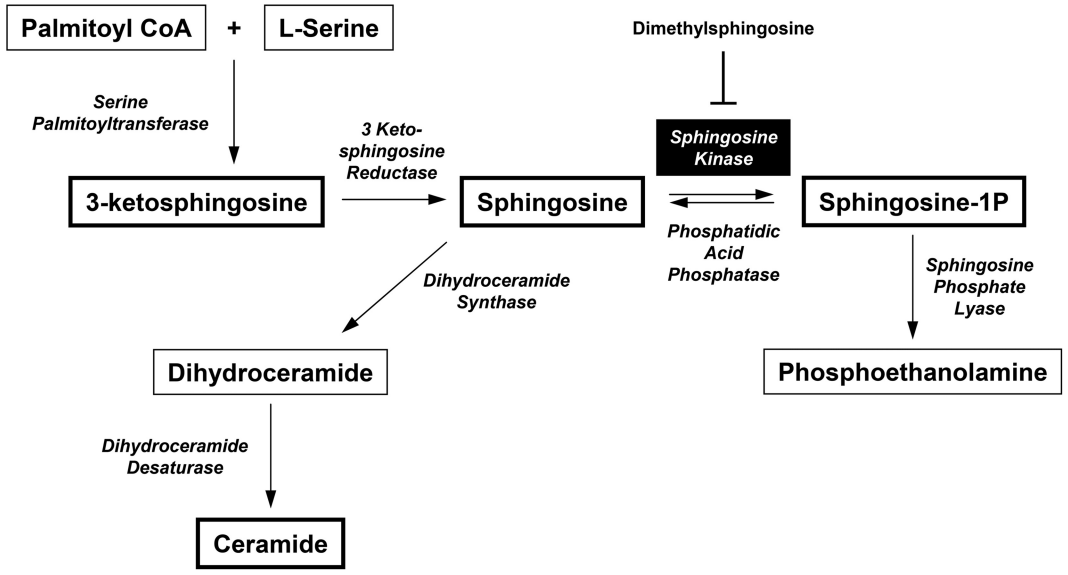

FIG 1 Sphingolipid metabolic pathway. The *de novo* biogenesis of sphingolipids begins with the condensation of serine and palmitoyl CoA by SPT. Bioactive sphingolipids (heavily outlined boxes), generated *de novo* or via breakdown of sphingomyelin, function as potent regulators of cellular proliferation and survival. Ceramide and sphingosine promote cell cycle arrest and apoptosis, while S1P, produced by phosphorylation of sphingosine by sphingosine kinase, promotes cell proliferation and survival. Sphingosine phosphate lyase catalyzes the irreversible cleavage of S1P to phosphoethanolamine, facilitating movement of bioactive sphingolipids into the ethanolamine biosynthesis pathway. Sphingosine may also be converted to dihydroceramide and then to ceramide, through the actions of dihydroceramide synthase and desaturase, respectively. Enzymes are italicized in this figure.

ceptors have not been identified in *T. brucei*, and MAPK orthologues have not been implicated in G_1/S-phase progression, suggesting an involvement of alternative pathways for trypanosome cell cycle regulation (9). As such, these alternative regulatory pathways may be amenable to targeting for trypanocidal therapy.

Compared with other eukaryotic cells, trypanosomes have multiple unique subcellular features, specifically the flagellum and a single mitochondrion harboring the kinetoplast mitochondrial DNA (kDNA), adding complexity to the *T. brucei* cell cycle, which is coordinated by microtubule morphogenesis (10). *T. brucei* begins the cell cycle with basal body duplication and nucleation of a new flagellum, followed by duplication of the kDNA and nuclear genome (11). Synthesis of kDNA coincides with initiation of nuclear DNA synthesis and rotation of the new basal body from an anterior to a posterior position relative to the old flagellum (12–14). While centrosomes are absent from trypanosomes, microtubule organizing centers, known as basal bodies, nucleate the flagellum but are not involved in spindle assembly (15). In fact, rotation of the basal body drives the segregation of the replicated kDNA (14, 16). Posterior-end repositioning of the duplicated basal body and kDNA occurs simultaneously with the initiation of mitosis (11, 13). Following mitosis, cytokinesis occurs as the cell divides longitudinally by binary fission along a cleavage furrow initiated at the anterior tip of the new flagellar attachment zone (17). The flagellum and attachment zone define the cleavage plane, which ingresses unidirectionally along the long axis from the anterior to the posterior end of the cell (18, 19).

Sphingolipids, or glucosylceramides, and their metabolites, ceramide, sphingosine and sphingosine-1-phosphate (S1P), contribute to eukaryotic plasma membrane architecture, function in protein trafficking and sorting (20, 21), and serve as second messengers for diverse cellular processes, including the heat stress response, regulation of cell growth, cell cycle progression, and apoptosis (22, 23). In trypanosomes, sphingolipids are synthesized through the condensation of palmitoyl coenzyme A (CoA) with serine, catalyzed by serine palmitoyltransferase (SPT) to form 3-ketosphingosine (Fig. 1). 3-Ketosphingosine is then modified reversibly to sphingosine, which is reversibly monophosphorylated by sphingosine kinase (SPHK) into S1P. As second messengers in eukaryotes, ceramide and sphingosine promote cell cycle arrest and apoptosis, while S1P promotes cell proliferation and survival (24–26). S1P can be dephosphorylated by phosphatidic acid phosphatase (PPAP) back into sphingosine. An alternative sphingosine pathway feeds into the ethanolamine biosynthesis pathway via irreversible cleavage of S1P by sphingosine phosphate lyase to produce phosphoethanolamine.

Sphingosine kinase (SPHK) is a highly conserved enzyme in eukaryotes. There are two isoforms in mammals, SPHK1 and SPHK2 (25). In humans, dysregulation of SPHK1 and its enzymatic product, S1P, leads to cancer cell survival and tumor progression (25), while in the protozoan *Leishmania*, SPHK is essential for viability and host cell infection (27).

A long-term goal of our laboratory is the development of novel drugs that specifically target trypanosomes while sparing the human (and animal) host. We previously discovered that SPT, a key enzyme in the ceramide biosynthetic pathway, is essential in *T. brucei* (28). Depletion of SPT2 results in substantially reduced levels of inositolphosphorylceramide and incomplete cleavage furrow formation, promoting aberrant cytokinesis and polyploidy (28). In the present study, we explored the function of SPHK in trypanosomes, with a focus on its involvement in cell cycle regulation. Through RNA interference (RNAi)-mediated depletion of *T. brucei* SPHK (TbSPHK) in insect procyclic-form (PF) *T. brucei*, we observed attenuated cell division, microtubule elongation at the posterior tip, and altered organelle positioning. Cytotoxicity

assays using TbSPHK inhibitors revealed a favorable therapeutic index between *T. brucei* and human cells.

RESULTS

Identification and confirmation of *T. brucei* SPHK. To identify SPHK orthologues in the *T. brucei* genome, a protein BLAST search was performed using the amino acid sequence for human SPHK1 (HsSPHK1; GeneID 8877) against *T. brucei* genome databases (http://www.genedb.org and http://www.tritrypdb.org). A single SPHK orthologue was identified (Tb927.7.1240), annotated as a putative SPHK having a conserved diacylglycerol kinase domain (C5). TbSPHK encodes a 769-amino-acid protein displaying 39 to 44% domain sequence identity with other trypanosomatid SPHKs and 21% domain identity with the human enzyme (Fig. 2). The analysis also revealed that TbSPHK contains a protein kinase domain (subdomains C1, C2, and C3), a sphingosine binding site (domain C4), and a lipid kinase domain (domain C5). In contrast to the HsSPHKs, the trypanosomatid SPHKs have more-extended protein kinase domains, suggesting potential differences in biochemical properties and/or substrate specificity. The N termini of the trypanosomatid enzymes are also considerably longer than those of the human enzymes.

TbSPHK activity decreases in growth-arrested cells. Consistent with the published transcriptome analysis (29), we found that TbSPHK is constitutively expressed in the log (L) and stationary (S) phases of both mammalian bloodstream-form (BF) and insect procyclic-form (PF) *T. brucei* (Fig. 3A). Similar to the results of the genome-wide transcriptome analysis previously performed (30), the SPHK mRNA level is greater in BF than in PF cells. To confirm that *T. brucei* can convert sphingosine to S1P, a defining activity of TbSPHK, whole-cell lysates were prepared from BF and PF trypanosomes for *in vitro* sphingosine kinase assays (Fig. 3B). TbSPHK converts sphingosine to S1P with Michaelis-Menten kinetics, with a 2.2-fold-greater specific activity in log-phase PF cells than in BF cells (83.1 ± 8.6 versus 37.4 ± 4.6 pmol · min^{-1} · mg^{-1}) at a saturating sphingosine concentration of 120 μM. TbSPHK activity in BF cells was attenuated 2-fold by the addition of the sphingosine kinase inhibitor dimethyl sphingosine (DMS). Similar to observations in *Saccharomyces cerevisiae* (31), SPHK activity is much lower in stationary-phase trypanosomes than in those in log phase. A 16.3- and an 8.9-fold decrease in activity were observed in stationary-phase PF (5.1 ± 0.7 pmol · min^{-1} · mg^{-1}) and BF (4.2 ± 1.4 pmol · min^{-1} · mg^{-1}) trypanosomes, respectively, compared to the log phase.

TbSPHK-depleted cells exhibit attenuated growth and defective G_1/S cell cycle transition. To investigate the role of TbSPHK in *T. brucei* growth regulation, we employed TbSPHK RNAi to deplete the enzyme in PF cells (Fig. 4A). TbSPHK RNAi was induced by the addition of tetracycline, and the growth of wild-type (WT) and TbSPHK RNAi cells (with or without addition of tetracycline [+Tet or −Tet, respectively]) was monitored daily for 10 days. Compared to control cells (WT and −Tet), growth defects were apparent in TbSPHK-depleted cells beginning at day 4 post-RNAi induction; by day 10, there was a 2-log difference in cumulative growth (Fig. 4A). This is consistent with the growth defect observed on TbSPHK depletion in a high-throughput RNAi screen performed previously (32). Depletion of TbSPHK mRNA was confirmed by reverse transcription-PCR (RT-PCR) (Fig. 4B), and analysis of TbSPHK enzymatic activity on days 2, 4, 6, and 8 post-RNAi induction revealed an 87% decrease in activity by day 2 (Fig. 4C).

The growth defects observed in TbSPHK RNAi cells by day 5 post induction suggested a possible role of TbSPHK in cell cycle progression and/or apoptosis, as observed in other eukaryotes (33). To determine whether TbSPHK participates in cell cycle regulation, the DNA content of wild-type (log- and stationary-phase) and TbSPHK RNAi cells (+/−Tet) was analyzed by flow cytometry 6 days post-RNAi induction (Fig. 4D). As expected, wild-type stationary-phase cells (WT_S) accumulated in G_1 compared to wild-type log-phase cells (WT_L). Analysis of TbSPHK RNAi cells (+/−Tet) revealed a modest but significant attenuation of G_1/S-phase transition in TbSPHK-depleted (+Tet) cells ($P < 0.05$), albeit less than that observed in stationary-phase cells. The growth defect observed in TbSPHK-depleted cells was not attributable to a cytokinesis defect or apoptosis, since no accumulation of multinucleated cells or cell debris was observed in ungated histograms. Further, no aberrant forms were noted by direct microscopy. Consistent with this observation, there was no evidence of necrosis or apoptosis in TbSPHK-depleted cells when analyzed by flow cytometry after costaining with propidium iodide and annexin V (data not shown). To confirm that the growth defects in RNAi cells are attributable to TbSPHK depletion and not to a downstream effect on the ethanolamine pathway (Fig. 1), we engineered an RNAi line permitting depletion of sphingosine phosphate lyase (TbSPL, Tb927.6.3630). Log-phase growth was not affected by TbSPL depletion (Fig. 5), indicating that TbSPL is not essential for growth.

TbSPHK regulates microtubule morphogenesis and organelle positioning. Although TbSPHK-depleted cells do not develop gross cytokinetic defects, we examined the morphology of these cells to further explore the growth defect. Log-phase TbSPHK-depleted cells are elongated, similarly to stationary-phase cells (Fig. 6A). Length measurements of the posterior end (distance between the kDNA and posterior end of the cell) in wild-type (log- and stationary-phase) and TbSPHK RNAi (+/−Tet) cells on day 6 postinduction revealed a significant ($P < 0.001$) increase in the posterior-end length of TbSPHK-depleted cells over that in control cells (Fig. 6B). TbSPHK-depleted cells exhibited a median posterior length of 6.2 μm, while wild-type log-phase and uninduced (−Tet) control cells exhibited median posterior lengths of 3.9 and 5.0 μm, respectively. Similarly to TbSPHK-depleted cells, wild-type stationary-phase cells have a median posterior-end length of 5.8 μm. With an upper quartile of 7.3 μm, extreme posterior lengths up to 13 μm were observed in TbSPHK-depleted cells, in which an upper quartile image is shown (Fig. 6A, XP). Notably, many TbPSHK-depleted cells exhibited abnormal kinetoplast positioning (Fig. 6A, KP).

To investigate a possible function for TbSPHK in regulating organelle positioning and cell morphology, we assessed microtubule assembly and nucleoid content in control and TbSPHK-depleted cells, staining the cells with anti-tyrosinated α-tubulin (YL1/2 [34]) to visualize basal bodies (B) and newly polymerized microtubules and 4′,6-diamidino-2-phenylindole (DAPI) to visualize kDNA (K) and nuclei (N) (Fig. 6A). An accumulation of tyrosinated α-tubulin was observed at the elongated posterior end of TbSPHK-depleted cells (Fig. 6A). This phenotype is irreversible. Removal of tetracycline and restoration of TbSPHK expression did not allow the cells to divide. As part of this elongation phenotype, the kinetoplast shifted to the posterior end of the cell,

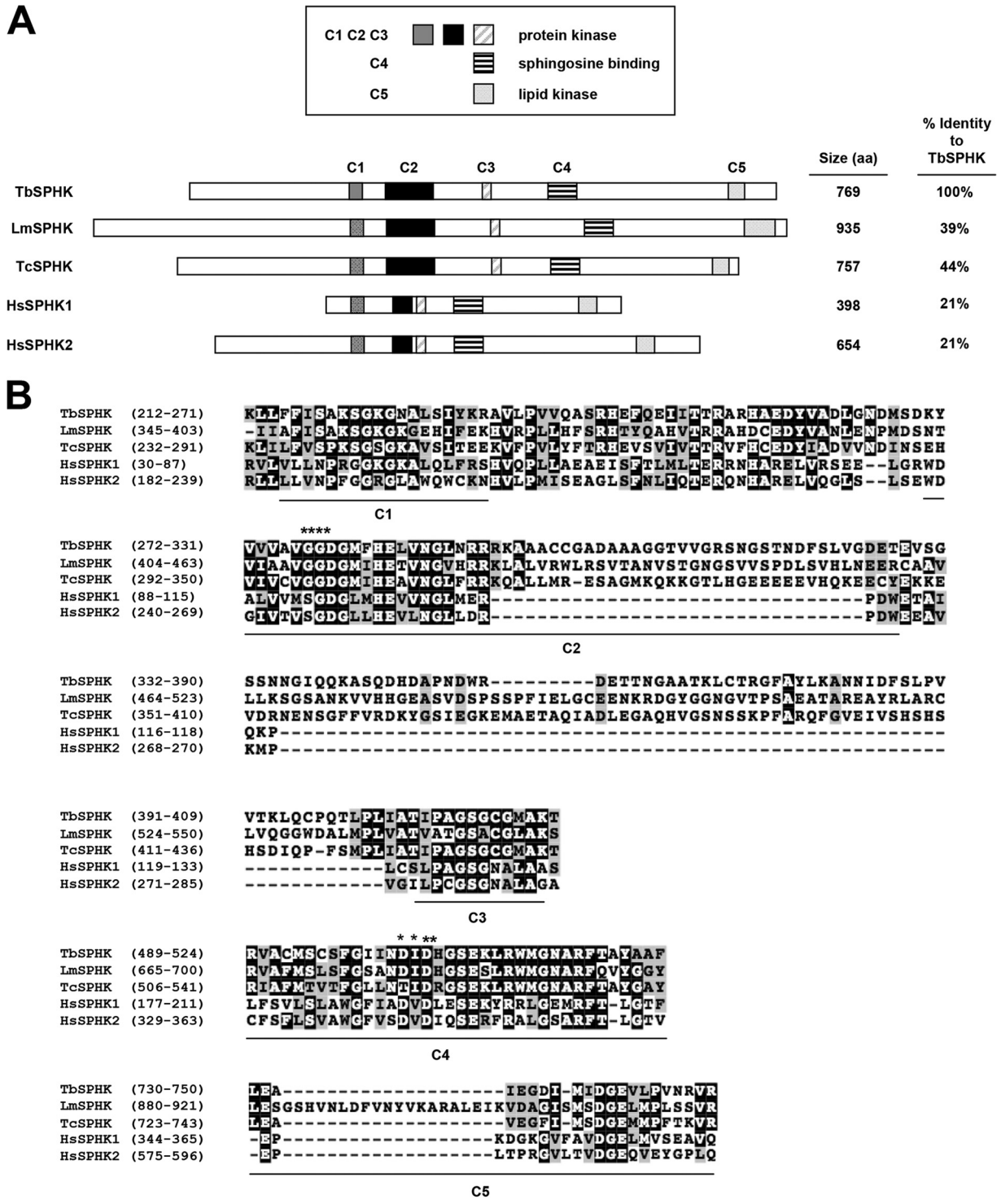

FIG 2 Conserved domain structure among SPHK orthologues. (A) Schematic of conserved domains found among SPHK orthologues in *T. brucei* (TbSHPK; Tb927.7.1240), *Leishmania major* (LmSPHK; LmjF26.0710), *Trypanosoma cruzi* (TcSPHK; Tc00.1047053507515.120), and *Homo sapiens* (HsSPHK1, Gene ID 8877; HsSPHK2, Gene ID 56848). TbSPHK harbors a conserved protein kinase motif (domains C1 to C3) and a sphingosine binding site (domain C4). Domain C5 is conserved among lipid kinases. Percent identity over the conserved domains is shown. aa, amino acids. (B) ClustalW multiple sequence alignment of the conserved domains (underlined) found in the SPHK orthologues described above. TbSPHK harbors a conserved protein kinase motif (domains C1 to C3) and sphingosine binding site (domain C4; asterisks). Asterisks above domain C2 denote the ATP-binding site. Domain C5 is a conserved domain observed among lipid kinases. Shading was generated by BOXSHADE (identical residues are shaded black, and conserved residues are shaded gray).

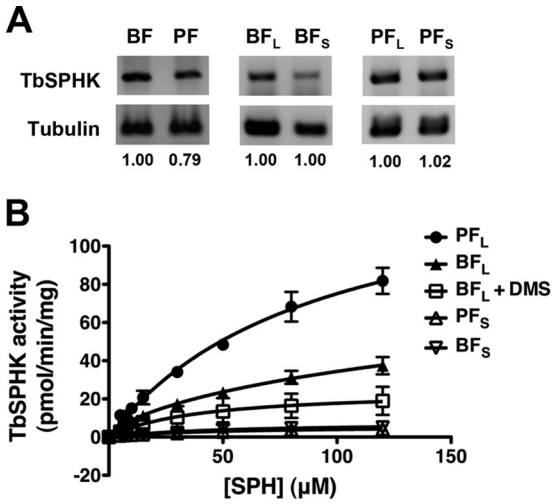

FIG 3 TbSPHK activity is attenuated in stationary phase. (A) Semiquantitative RT-PCR analysis of TbSPHK expression in log- and stationary-phase bloodstream-form (BF) and procyclic-form (PF) trypanosomes. Values represent relative TbSPHK expression after normalization to tubulin. Representative results from triplicate experiments are shown. (B) Analysis of TbSPHK enzymatic specific activity in log- and stationary-phase BF and PF trypanosomes. *In vitro* sphingosine kinase assays were performed in the presence of [γ-^{32}P]ATP (10 μCi), 0 to 120 μM sphingosine, and 10 μg whole-cell extracts, as described in Materials and Methods. For the analysis of DMS inhibitor kinetics in BF trypanosomes, assays were performed in the absence or presence of 10 μM DMS (K_i = 1.05 ± 0.15 μM). Lipids were extracted and resolved by TLC, and radiolabeled S1P was quantified by phosphorimaging, followed by nonlinear regression. Data are expressed as means ± standard deviations from triplicates of three independent experiments.

accompanied by concentration of tyrosinated α-tubulin at the extended posterior tip. Flagellar length increased commensurate with cell elongation. Nucleoid analysis of TbSPHK-depleted cells showed a modest but significant accumulation of 1B1K1N cells (Fig. 6C), compared to control cells, confirming the attenuation of G_1/S-phase cell cycle progression observed by flow cytometry (Fig. 4D).

The *T. brucei* cell cycle is highly coordinated and mediated by microtubule dynamics that ensure correct duplication and segregation of organelles at all life cycle stages (10, 12, 14, 16). When procyclic trypanosomes in the tsetse midgut differentiate to proventricular epimastigotes, the cells elongate, arrest in G_0/G_1, $G_0$and reposition the kinetoplast from posterior to anterior relative to the nucleus (35). Since it appears that TbSPHK functions upstream of microtubule morphogenesis or patterning (Fig. 6A and B), which is in turn responsible for proper organelle positioning, the 1B1K1N cells (Fig. 6A) were further analyzed for kDNA positioning (Fig. 6D). TbSPHK depletion resulted in mispositioning of the basal body/kinetoplast anterior to the nucleus position in 27.7% ± 2.7% of cells versus 0.5% ± 0.9%, 4.3% ± 2.7%, and 2.5% ± 0.9% of wild-type log-phase cells, wild-type stationary-phase cells, and uninduced RNAi controls, respectively (Fig. 6A and C). This finding further supports a role for TbSPHK in microtubule assembly and organelle positioning and suggests a possible role of SPHK in the differentiation of trypanosomes from procyclic to mesocyclic forms. Beyond these cellular changes, overall morphology and microtubule organization appear normal.

SPHK inhibitors kill *T. brucei in vitro*. To evaluate TbSPHK as a potential therapeutic target, we tested the SPHK inhibitors dimethylsphingosine (DMS) (36) and L-threodihydrosphingosine (safingol) (37) on the viability of *T. brucei* BF cells (Fig. 7). Mammalian cell growth inhibition was assessed in parallel using human U937 histiocytic lymphoma cells to model a rapidly growing human cell likely to be sensitive to systemic cell cycle inhibitors. Cell viability in the presence of vehicle or various concentrations of the indicated SPHK inhibitor was measured 24 h posttreatment using the thiazolyl blue tetrazolium bromide (MTT) assay of cell viability (Fig. 7). Both DMS and safingol demonstrated a wide therapeutic index of cytotoxicity between BF *T. brucei* (50% lethal concentration [LC_{50}] = 1 to 1.5 μM for both DMS and safingol) and human U937 cells (DMS LC_{50} = >12.8 μM; safingol LC_{50} = 16 to 20 μM).

DISCUSSION

In eukaryotes, sphingolipids play important roles in cell membrane structure, signal transduction, and protein trafficking. Sphingolipids are also essential for the viability and virulence of the trypanosomatid *Leishmania* (27). SPHK, which phosphorylates sphingosine to generate S1P, regulates a number of important cellular processes, such as proliferation, apoptosis, calcium homeostasis, and the immune response (24). While most eukaryotes possess two SPHK isoforms, trypanosomatids have only one (Fig. 2). Differences in domain sequence and length between trypanosomatid and human SPHK proteins (Fig. 2) suggest biochemical differences that may afford an avenue for drug discovery for these important human pathogens.

We previously discovered that SPT is essential in *T. brucei* (28). SPT depletion prevented the synthesis of inositolphosphorylceramide, leading to defective cytokinesis and the production of multinucleated, multiflagellated syncytia which then die. To continue this work on lipid synthesis pathways, we investigated the role of SPHK in trypanosome physiology (Fig. 1). TbSPHK is constitutively expressed in both log- and stationary-phase BF and PF cells, with higher mRNA levels in BF cells (Fig. 3). Study of TbSPHK enzymatic activity revealed typical Michaelis-Menten kinetics, which was significantly attenuated in stationary-phase cells. This is consistent with findings in yeast, in which higher SPHK specific activity is observed during log-phase growth (30). Furthermore, a 2.2-times-greater TbSPHK specific activity was observed in PF than in BF cells. Therefore, while TbSPHK is constitutively expressed, TbSPHK enzymatic activity is differentially regulated, both during the cell cycle and in different life cycle stages of *T. brucei*.

The observation that TbSPHK activity is differentially regulated in the *T. brucei* cell and life cycles prompted us to investigate the effect of TbSPHK depletion on cell viability. TbSPHK RNAi resulted in a growth defect that began to be apparent at 4 days post-RNAi, almost certainly because it took several days for TbSPHK protein levels to drop low enough for the deficiency to be expressed. Cumulative growth was 2 logs lower by day 10 post-RNAi induction (Fig. 4). However, no accumulation of aberrant karyotypes was observed as assessed by flow cytometry (Fig. 4D) or immunofluorescence microscopy (Fig. 6C), indicating that TbSPHK is not required for proper cytokinesis. Growth impairment in SPHKA-knockout cells was noted in *Leishmania* promastigotes as well (27), suggesting pleiotropic effects of SPHK depletion across kinetoplastids.

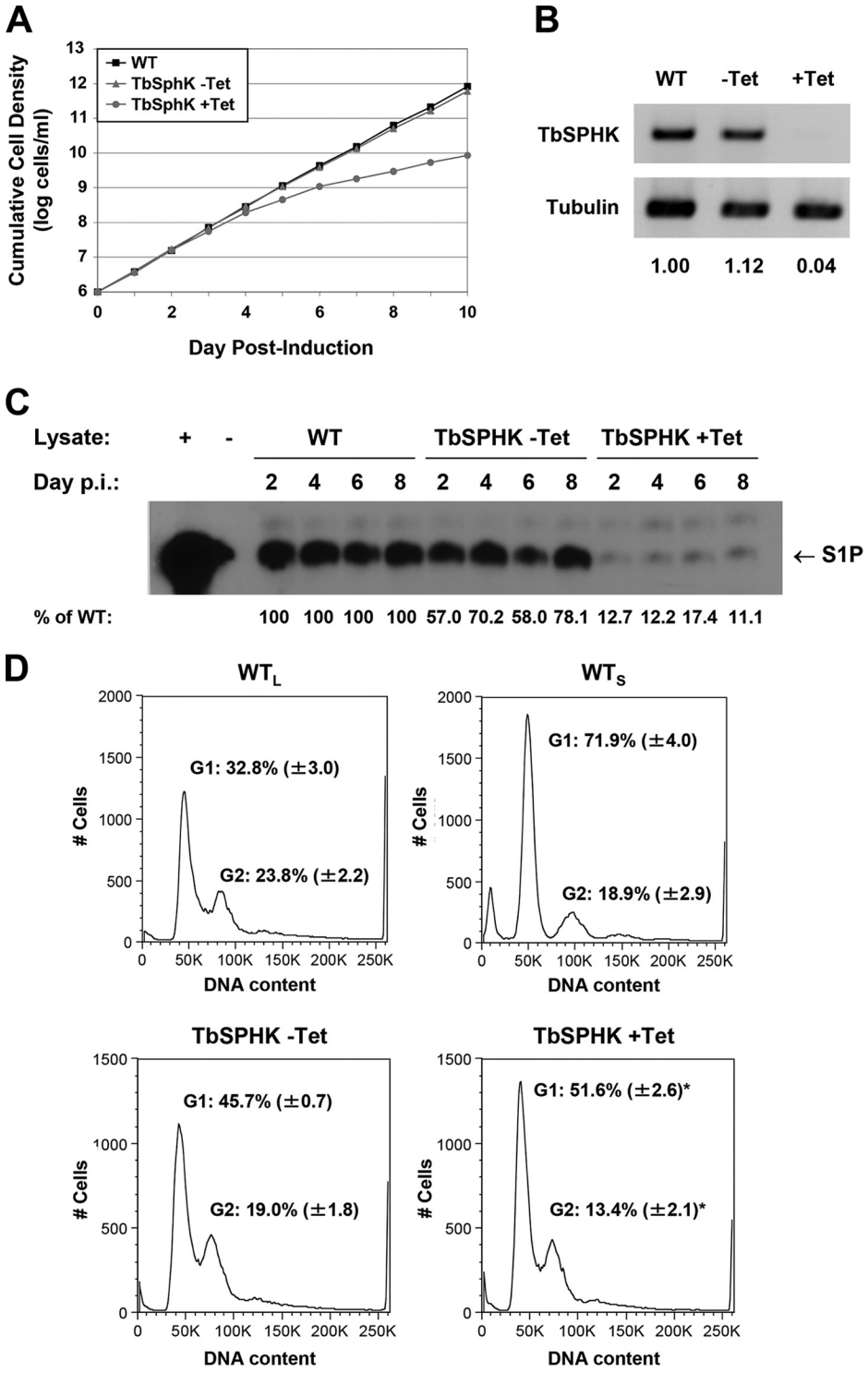

FIG 4 TbSPHK-depleted cells exhibit attenuated growth and accumulation in G_1/S. (A) Cumulative cell growth of PF wild-type (WT), uninduced (−Tet), and tetracycline-induced (+Tet) TbSPHK RNAi cells. Data are expressed as means of triplicates from three independent experiments ± standard deviations. (B) Semiquantitative RT-PCR analysis of TbSPHK expression in BF, PF, and TbSPHK RNAi-induced cells on day 2 postinduction. Values represent relative TbSPHK expression after normalization to tubulin. (C) Effect of TbSPHK depletion on endogenous sphingosine kinase activity. *In vitro* sphingosine kinase assays were performed in the presence of [γ-^{32}P]ATP (10 μCi), sphingosine (15 μM), and whole-cell extracts (10 μg) isolated from wild-type, uninduced, and tetracycline-induced TbSPHK RNAi cells on days 2, 4, 6, and 8 postinduction (p.i.). Control reactions were performed in the presence of recombinant His-HsSPHK1 (+) or heat-inactivated wild-type whole-cell extract (−). Lipids were extracted and resolved by TLC, and radiolabeled S1P was quantified by phosphorimaging. (D) Cell cycle analysis of wild-type log (WT_L)- and stationary (WT_S)-phase cells and TbSPHK RNAi cells grown in the presence or absence of tetracycline (+Tet or −Tet, respectively) for 6 days. Cells (10^7) were stained with propidium iodide, and DNA content was determined by flow cytometry and analyzed using ModFit software. Representative histograms from triplicate experiments are shown. Mean percentages (± standard deviations) of G_1- and G_2-phase parasites are shown (*, $P < 0.05$). Representative results from triplicate experiments are shown in panels C and D (± standard deviations).

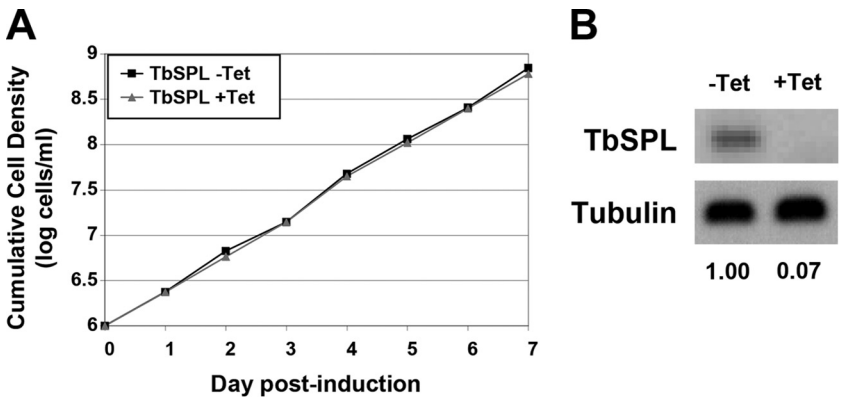

FIG 5 *T. brucei* sphingosine-1-phosphate lyase is not essential for growth. (A) Cumulative cell growth of PF control (−Tet) and tetracycline-induced (+Tet) TbSPL RNAi cells. (B) Semiquantitative RT-PCR analysis of TbSPL expression in control and TbSPL RNAi-induced cells on day 2 postinduction. Values represent relative TbSPL expression after normalization to a tubulin control.

To dissect the basis for growth impairment, we analyzed parasite DNA content, reflective of the cell cycle stage of the parasite, and observed that TbSPHK-depleted cells accumulated in G_1. This suggests that cell cycle delay is central to the growth deficit. Given the essential role of microtubule dynamics in cell division, we analyzed cells for the distribution of newly polymerized tyrosinated α-tubulin in TbSPHK-depleted cells, which revealed both an accumulation of tubulin and an elongation of the posterior end of the cell, as well as kinetoplast mispositioning (Fig. 6). Previous work by Gourguechon et al. also revealed an elongated posterior end in *T. brucei* cells depleted of cyclin E1 plus CR2 (6). This posterior-end elongation phenotype had previously been named "nozzle" by the Matthews group, when they observed the same result from zinc finger protein TbZFP2 overexpression (38). RNAi depletion of PHO80-like cyclin CYC2 also produced nozzle cells (39). Similarly to TbZFP2 overexpression and CYC2 RNAi cells, the microtubule extension in TbSPHK-depleted cells was a regulated process focused at the posterior tip of the cell body. The timeline for the appearance of the phenotype in the case of TbSPHK knockdown was similar to that observed upon CYC2 depletion. Importantly, accumulation of tyrosinated tubulin is not observed in elongated stationary-phase wild-type cells, which naturally exhibit attenuated TbSPHK activity (Fig. 3). This could be attributed to a dose-dependent contribution of SPHK to this process or perhaps altered environmental signaling during periods of limited nutrient availability. It is also noteworthy that the TbSPHK cells, once they become nozzle cells, remain so even after release of TbSPHK inhibition and die. We also ruled out the possibility that the nozzle phenotype developed as a result of a downstream effect on the ethanolamine pathway, by depleting TbSPL (Fig. 1). Knockdown of TbSPL had no effect on growth or cell morphology (Fig. 5).

The abnormal microtubule dynamics led us to examine the positions of the nucleus, kinetoplast, and basal bodies. Normally, posterior movement of the duplicated basal bodies and kDNA accompanies the initiation of mitosis, while rotational movements of basal bodies help drive segregation of the newly replicated kDNA (6–8). Analysis of TbSPHK-depleted cells revealed defects in basal body and kDNA positioning without production of aberrant nucleus and kDNA content. Together, these findings suggest that SPHK plays a role in microtubular patterning and organelle positioning which, while not essential, contributes to attenuated cell growth by cell cycle arrest in G_1. Since canonical growth factor receptors are absent from *T. brucei* and mitogen-activated protein kinase (MAPK) orthologues are not involved in G_1/S-phase progression (9), trypanosomes may have evolved distinct mechanisms regulating these processes (9). Thus, S1P, the product of TbSPHK enzymatic activity, may have a unique role in trypanosome cell cycle progression, different from that in higher eukaryotes.

In addition to becoming nozzle cells, TbSPHK-depleted cells also exhibit a repositioning of the kinetoplast from a posterior to an anterior position relative to the nucleus, suggesting possible involvement of TbSPHK inhibition in the differentiation of procyclic forms to mesocyclic forms. When the nozzle phenotype was first reported upon depletion of the CCCH proteins ZFP1 and ZFP2, differentiation of BF to PF cells was inhibited (38). It is yet to be determined if all the proteins whose depletion causes the nozzle phenotype work independently or together through one or more pathways, some of which could also be involved in regulating cell differentiation. Nonetheless, the resemblance of the posterior-end length of TbSPHK-depleted cells to wild-type stationary-phase cells, in addition to modest attenuation of TbSPHK-depleted cells in G_1/S-phase cell cycle transition (Fig. 4C), suggests that S1P modulates an upstream cellular process indirectly affecting cell cycle progression and procyclic differentiation. This is the first report that links sphingolipid metabolism to trypanosome cell cycle regulation and differentiation.

The results of cytotoxicity assays with SPHK inhibitors (Fig. 7) suggest that TbSPHK may be a novel drug target. Both DMS and safingol have a 10-fold therapeutic index versus human cells. DMS is useful for the treatment of neuropathic pain in rats (40), and safingol is currently in clinical trials for relapses of solid tumor malignancies (https://clinicaltrials.gov/ct2/show/NCT01553071). If eventually approved for use in humans, both of these drugs could be tested for repurposing to treat *T. brucei* infection. Since most eukaryotes have two SPHK isoenzymes and trypanosomes have one, it is possible that mammalian cells are more tolerant to SPHK inhibitors than are trypanosomes. Recent studies suggest redundancy in the function of the two isoenzymes, as homozygous single knockouts are viable with no obvious phenotypes in either yeast (41) or mice (42, 43). Research in HeLa cells also

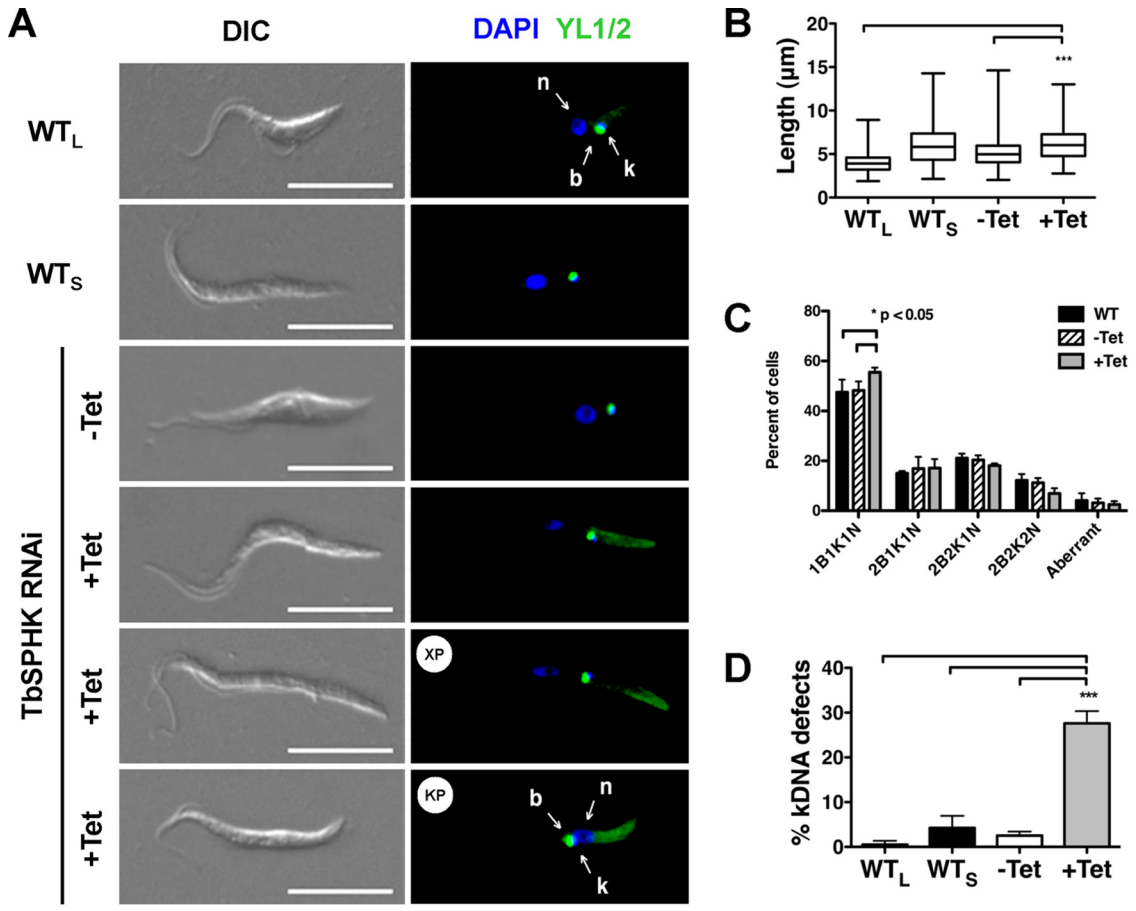

FIG 6 TbSPHK regulates posterior morphology and organelle positioning. (A) Wild-type log-phase (WT_L), wild-type stationary-phase (WT_S), and TbSPHK RNAi (+Tet or −Tet) cells were stained with DAPI (DNA) and YL1/2 (tyrosinated tubulin/basal bodies) and analyzed by immunofluorescence microscopy on day 6 postinduction. Arrows indicate the positions of the nucleus (n), kDNA (k), and basal bodies (b). Representative images of median 1B1K1N cell posterior lengths are shown. The cells at the bottom marked XP and KP represent those having extreme posterior elongation and abnormal kDNA positioning, respectively. Bar, 10 μm. DIC, differential interference contrast. (B) Quantification of extended posterior-end morphology in 1K1N wild-type (log- and stationary-phase) and TbSPHK RNAi-uninduced (−Tet) and induced (+Tet) cells showing minimum, mean, and maximum posterior-end lengths on day 6 postinduction. Measurements were taken between the kDNA and posterior end (>150 1B1K1N cells per group) using AxioVision software, and data were analyzed by one-way ANOVA, followed by Bonferroni posttest. Data are expressed as means ± standard deviations. ***, $P < 0.001$. (C) Karyotype analysis of TbSPHK RNAi-depleted cells grown in the absence or presence of tetracycline for 6 days. Cells were costained with DAPI and YL1/2 antibody, and nuclei, kinetoplasts, and basal bodies were assessed microscopically. Cell nuclear and kinetoplast contents were scored manually, and data were analyzed by two-way ANOVA, followed by the Bonferroni posttest. Mean percentages (± standard deviations) of 1B1K1N, 2B1K1N, 2B2K1N, 2B2K2N, and aberrant cells ($n > 200$) from triplicate experiments are shown (*, $P < 0.05$). (D) Percentages of cells showing kDNA positioning defects in log- and stationary-phase wild-type (1B1K1N) cells and in TBSPHK RNAi cells induced or not by tetracycline (+Tet or −Tet, respectively). A mispositioned basal body/kinetoplast is located anterior to the nucleus (toward the free flagellum, left in this panel). Data (± standard deviations) were analyzed by one-way ANOVA, followed by the Bonferroni posttest (***, $P < 0.001$).

indicates a role for HsSPHK1 in endocytic membrane trafficking (44), an area that needs further investigation in other organisms, including trypanosomes. Taken together, our work and the work of others suggests that TbSPHK may be a novel target for trypanocidal chemotherapy. Further studies of S1P function in trypanosomes are needed to elucidate its diverse function in various cellular activities, including the cell cycle regulation and differentiation of procyclic forms to mesocyclic forms.

Finally, our findings highlight the importance of lipid metabolic pathways in regulating cellular and molecular processes. Within the realm of sphingolipids, future studies on the sphingolipid metabolic pathway and direct targets of S1P would advance our understanding of the mechanisms by which SPHK regulates *T. brucei* cell cycle regulation. Of course, this is always the challenge with results like these—how to link a metabolic enzyme to major aberrations in cell morphology, in this case microtubule dynamics, organelle positioning, and cell cycle regulation. Characterization of additional enzymes involved in sphingolipid metabolism will not only improve our understanding of trypanosome biology but also expand knowledge of signaling pathways affected by modified sphingosines.

MATERIALS AND METHODS

Cell culture. All *T. brucei* cells developed for this study were derived from the PF 29-13 line or the bloodstream-form (BF) "single marker" line (45). Both were originally derived from Lister strain 427, antigenic type MITat1.2, clone 221a (46), and were engineered to coexpress bacteriophage T7 RNA polymerase and tet repressor to permit tetracycline-inducible transcription. PF parasites were cultured at 27°C in SDM-79 medium (47) supplemented with 10% dialyzed fetal bovine serum (FBS; Sigma-Aldrich, Saint Louis, MO), 7.5 μg/ml hemin, 100 U/ml penicillin-

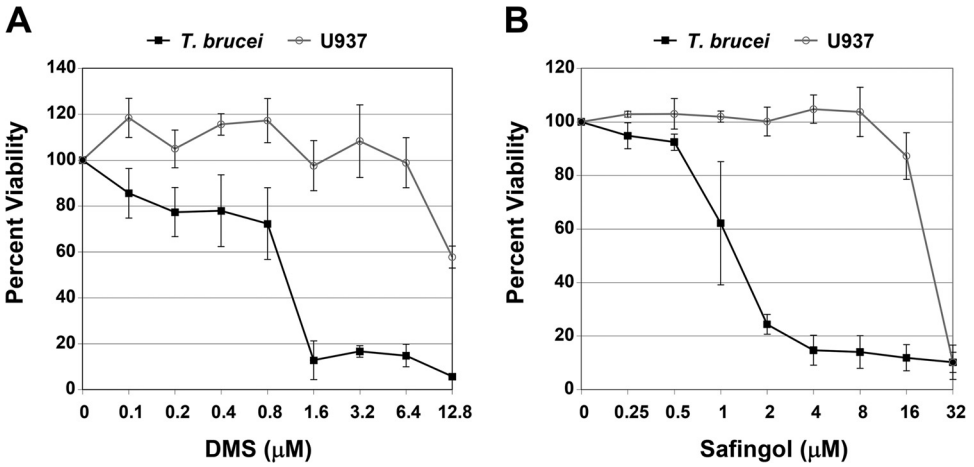

FIG 7 Sphingosine kinase inhibitors are toxic to *T. brucei* in vitro. Bloodstream-form *T. brucei* or U937 myeloid leukemia cells (control) were treated for 24 h with vehicle or the indicated concentrations of DMS or safingol, and cell viability was determined using the MTT assay. Data showing mean percent viability (± standard deviation) from triplicates of three independent experiments are shown.

streptomycin, 50 μg/ml hygromycin, and 15 μg/ml G418. BF parasites were cultured at 37°C with 5% CO_2 in HMI-9 medium (47) supplemented with 10% FBS, 10% serum plus medium complement (SAFC Biosciences, Lenexa, KS), 100 U/ml penicillin-streptomycin, and 2.5 μg/ml G418. RNAi cell lines were cultured under continuous drug selection with 2.5 μg/ml phleomycin. U937 human leukemic monocytes (ATCC) (48) were cultured at 37°C with 5% CO_2 in RPMI 1640 medium (Invitrogen, Carlsbad, CA) supplemented with 10% FBS.

Generation of RNAi constructs and cell lines. For the generation of TbSPHK RNAi mutants in PF *T. brucei*, a unique 532-bp region of the TbSPHK locus (Tb927.7.1240), identified by RNAit software (49), was amplified from 29-13 genomic DNA using primers GGCCTCGAGATTC CAGCTGGTAGTGGGTG (5′ SPHK containing an XhoI linker [underlined]) and GGCAAGCTTGGCACTGATCCGTGTATGTG (3′ SPHK reverse primer containing a HindIII linker [underlined]). The PCR product was digested with XhoI and HindIII, subcloned into the pZJM RNAi vector (50), and sequenced. For the generation of pZJM-TbSPL, a 519-bp fragment of TbSPL (Tb927.6.3630) was amplified from 29-13 genomic DNA using primers CGATGGTCGTTCACATGTTCAACG (5′ SPL forward) and CCTTTGGGAGCAAAACCATACTTGTG (3′ SPL reverse) and subcloned into the pCR-BLUNTII-TOPO vector (Invitrogen, Carlsbad, CA) before digestion with XhoI and HindIII and ligation into pZJM.

For transfection of PF *T. brucei*, 10 μg of NotI-linearized pZJM-TbSPHK or pZJM-TbSPL DNA (or water control) was mixed with 2.25 × 10^7 29-13 cells suspended in 450 μl of electroporation medium (120 mM KCl, 0.15 mM $CaCl_2$, 9.2 mM K_2HPO_4, 25 mM HEPES, 2 mM EDTA, 4.75 mM $MgCl_2$, 69 mM sucrose, pH 7.6), transferred to a 0.4-cm-gap cuvette, and electroporated twice at 1.4 kV, 25 μF, using a Bio-Rad Gene Pulser electroporator (Bio-Rad, Hercules, CA). Cells were transferred to 10 ml of fresh SDM-79 medium, and antibiotic selection was initiated 24 h posttransfection by the addition of 2.5 μg/ml phleomycin. RNAi induction was initiated with the addition of 1 μg/ml tetracycline, and RNA was isolated with 1 ml Trizol reagent (Invitrogen, Carlsbad, CA) per 10^8 cells on day 2 postinduction.

Determination of RNAi effectiveness was performed via RT-PCR using cDNA prepared from total RNA (2 μg) by reverse transcription using GAGAATTCTCGAGTCGACTTTTTTTTTTTTTTTT [oligo(dT)-RXS primer] and the SuperScript III first-strand synthesis system (Invitrogen, Carlsbad, CA), as described by the manufacturer. 29-13::pZJM-TbSPHK-positive clones were validated by semiquantitative RT-PCR using primers CACATACACGGATCAGTGCC (SK-IntF) and CGGGATCCGCGGCCGC CTACTTCCCAGGCAAACTCAGG (pGEX-SPHK-rev). 29-13::pZJM-TbSPL-positive clones were validated by semiquantitative RT-PCR using AGTGCCGAAGGCATAAAGATGCCG (TbSPL-RTfor) and ATGCTCTC-CATGATACACTGCGCC (TbSPL-RTrev). Relative TbSPHK and TbSPL mRNA levels were normalized to α-tubulin mRNA using primers TGTTCT TGGACCTGGAGCCAACAGT (α-tubulin RT-PCR forward) and TAGCC GAGCTTGGACTTCTTGCCA (α-tubulin RT-PCR reverse).

***In vitro* growth curves.** Wild-type 29-13 and TbSPHK RNAi cells were seeded at an initial density of 10^6 cells/ml, and RNAi induction was initiated by the addition of 1 μg/ml tetracycline. Cell density was monitored daily using a Z-series Coulter Counter with a lower threshold set to 3 μm and an upper threshold set to a 10-μm diameter. Cultures were diluted to 10^6 cells/ml with fresh medium every 2 days to maintain parasites in the logarithmic phase of growth.

***In vitro* sphingosine kinase assays.** Whole-cell extracts were prepared by sonication (10 s at 20% amplitude over a 20-s interval using a Branson sonicator [Danbury, CT]) in assay buffer (0.1 M Tris-HCl [pH 7.4], 10 mM magnesium chloride, 1 mM EGTA, 15 mM sodium fluoride, 1 mM sodium orthovanadate, 1 mM dithiothreitol, 0.5 mM 4-deoxypyridoxine) containing 10% glycerol and 1× EDTA-free protease inhibitor tablet (Roche, Basel, Switzerland). Lysates were quantified alongside a bovine serum albumin (BSA) standard curve by spectrophotometry using the protein assay reagent (Bio-Rad, Hercules, CA) and diluted to 0.2 mg/ml with assay buffer containing 10% glycerol and a protease inhibitor cocktail. *In vitro* sphingosine kinase assays (100-μl volume) were performed for 30 min at 37°C as described elsewhere (37) with the following modifications. For the analysis of enzyme and inhibitor kinetics, assays were performed in the presence or absence of 10 μM *N*,*N*-dimethylsphingosine (dissolved in 5% Triton X-100; Avanti Polar Lipids) in assay buffer containing 10 μCi [γ-^{32}P]ATP (specific activity, 3,000 Ci/mmol), 1 mM ATP, 10 μg whole-cell lysate, 0 to 120 μM D-erythrosphingosine (dissolved in 5% Triton X-100; Avanti Polar Lipids, Alabaster, AL), and a final 0.4% Triton X-100 concentration. For the analysis of TbSPHK activity exhibited by TbSPHK RNAi-depleted cells on days 2, 4, 6, and 8 postinduction, assays were performed as described above in the presence of 15 μM D-erythrosphingosine. Control reactions were performed as described above in the presence of 5 ng human recombinant SPHK1 (Cayman Chemical, Ann Arbor, MI; positive control) or 10 μg of heat-inactivated lysates (negative control) prepared by boiling at 100°C for 10 min. Reactions were terminated by lipid extraction with the addition of 270 μl chloroform-methanol-HCl (100:200:1, vol/vol). After vigorous vortexing, 70 μl of chloroform and 20 μl of 2 M KCl were added, and phases were separated by centrifugation. Twenty microliters of the organic phase was resolved by thin-layer chromatography (TLC) on silica gel G60 plates (Whatman, Maidstone, United Kingdom) using a 1-butanol–ethanol–

acetic acid–water mobile phase (80:20:10:20, vol/vol), and radiolabeled S1P was visualized using a Fujifilm FLA-5100 phosphorimager (Valhalla, NY). TbSPHK activity was expressed as picomoles per minute per milligram of protein after quantification of radiolabeled S1P alongside a [γ-^{32}P]ATP/ATP standard curve.

Flow cytometry. Cell samples for flow cytometric analysis were prepared as described elsewhere (51), with the following modifications. On day 6 postinduction, 1×10^7 wild-type (log and stationary) and TbSPHK RNAi (+/−Tet) cells were harvested by centrifugation (1,000 × *g* at 4°C for 10 min) and washed twice in phosphate-buffered saline (PBS). Cell pellets were fixed and permeabilized by suspension in 100 μl of PBS and mixed with 200 μl of PBS containing 10% ethanol and 5% glycerol. Cells were then mixed with 200 μl of PBS containing 50% ethanol and 5% glycerol and incubated on ice for 5 min. One milliliter of PBS containing 70% ethanol and 5% glycerol was then added, and cells were incubated at 4°C overnight. The cells were then harvested by centrifugation, washed twice in PBS, and suspended in PBS containing 10 μg/ml RNase A (Sigma-Aldrich, Saint Louis, MO), 50 μg/ml propidium iodide, and 0.1% Triton X-100. Following a 30-min incubation at 37°C, cells were put through a 40-μm cell strainer and analyzed by using a Becton, Dickinson LSRII flow cytometer and FACSDiva acquisition software (BD Biosciences, Franklin Lakes, NJ). For DNA analysis, cells (30,000 events per sample) were gated on 2N/4N DNA content, and cell cycle analysis was performed using ModFit software (Verity House Software, Topsham, ME).

Immunofluorescence microscopy. Parasites were pelleted by centrifugation at 1,000 × *g* for 10 min, washed twice in PBS supplemented with 13 mM glucose, fixed in 4% paraformaldehyde prepared in PBS, and allowed to settle onto poly-L-lysine-coated slides for 30 min on ice. Fixative was quenched with 50 mM glycine for 15 min. Cells were permeabilized with 0.2% Triton X-100 prepared in PBS for 15 min and incubated in blocking buffer (2% normal goat serum, 1% BSA in PBS) for 1 h. Cells were incubated overnight with rat anti-YL1/2 antibody (34) (provided by Keith Gull, Oxford University) diluted 1:10 in blocking buffer, followed by a 30-min wash with PBS. Samples were then incubated for 1 h in Alexa Fluor 488-conjugated goat anti-rat secondary antibody (Life Technologies, Carlsbad, CA) diluted 1:400 in blocking buffer and washed for 30 min with PBS. Cells were incubated with 1 μg/ml 4′,6-diamidino-2-phenylindole (DAPI) for 10 to 20 s, washed for 2 min with ultrapure water, and mounted with Gelvatol containing 100 mg/ml 1,4-diazabicyclo[2.2.2]octane. Imaging was performed on a Zeiss upright microscope (Peabody, MA) using a 100× objective. Image acquisition, deconvolution, and analysis were performed using AxioVision software (Peabody, MA).

SPHK inhibitors and cytotoxicity assays. For *in vitro* cytotoxicity assays, BF *T. brucei* or U937 human lymphoma monocytes were seeded to 5×10^5 cells/ml in 96-well plates and cultured for 24 h in the presence of 0 to 12.8 μM dimethylsphingosine (DMS) or 0 to 32.0 μM L-threodihydrosphingosine (safingol; Avanti Polar Lipids, Alabaster, AL) (0.1% final ethanol concentration). At 24 h posttreatment, cells were pelleted by centrifugation, suspended in 100 μl of fresh medium containing 1 mM thiazolyl blue tetrazolium bromide (MTT; Sigma-Aldrich, Saint Louis, MO), and incubated at 37°C for 4 h. After the addition of 100-μl solubilization solution (0.1 g/ml SDS prepared in 0.1 M HCl), cells were then incubated at 37°C overnight, and absorbance was measured at 540 nm with a reference wavelength of 690 nm.

Statistical analysis. Statistical analyses for TbSPHK enzymatic activity assays were performed via nonlinear regression using GraphPad Prism 5 software (La Jolla, CA). For cell karyotype comparisons and posterior-end length comparisons, two-way and one-way analyses of variance (ANOVAs), respectively, were used, followed by the Bonferroni posttest.

ACKNOWLEDGMENTS

We thank Keith Gull (Oxford University) for the YL1/2 antibody.

This work was supported in part by research grant R01-GM93359 from the National Institute of General Medical Sciences. D.A.P. was supported in part by training grant T32-AG00260 from the National Institute on Aging.

REFERENCES

1. **Stuart K, Brun R, Croft S, Fairlamb A, Gürtler RE, McKerrow J, Reed S, Tarleton R.** 2008. Kinetoplastids: related protozoan pathogens, different diseases. J Clin Invest **118:**1301–1310. http://dx.doi.org/10.1172/JCI33945.
2. **WHO.** 2014. World Health Organization: trypanosomiasis, human African (sleeping sickness). WHO, Geneva, Switzerland. http://www.who.int/mediacentre/factsheets/fs259/en/.
3. **Torr SJ, Hargrove JW, Vale GA.** 2005. Towards a rational policy for dealing with tsetse. Trends Parasitol **21:**537–541. http://dx.doi.org/10.1016/j.pt.2005.08.021.
4. **Tu X, Wang CC.** 2005. Coupling of posterior cytoskeletal morphogenesis to the G_1/S transition in the *Trypanosoma brucei* cell cycle. Mol Biol Cell **16:**97–105. http://dx.doi.org/10.1091/mbc.E04-05-0368.
5. **Li Z, Wang CC.** 2003. A PHO80-like cyclin and a B-type cyclin control the cell cycle of the procyclic form of *Trypanosoma brucei*. J Biol Chem **278:**20652–20658. http://dx.doi.org/10.1074/jbc.M301635200.
6. **Gourguechon S, Savich JM, Wang CC.** 2007. The multiple roles of cyclin E1 in controlling cell cycle progression and cellular morphology of Trypanosoma brucei. J Mol Biol **368:**939–950. http://dx.doi.org/10.1016/j.jmb.2007.02.050.
7. **Kumar P, Wang CC.** 2006. Dissociation of cytokinesis initiation from mitotic control in a eukaryote. Eukaryot Cell **5:**92–102. http://dx.doi.org/10.1128/EC.5.1.92-102.2006.
8. **Torii S, Yamamoto T, Tsuchiya Y, Nishida E.** 2006. ERK MAP kinase in G cell cycle progression and cancer. Cancer Sci **97:**697–702. http://dx.doi.org/10.1111/j.1349-7006.2006.00244.x.
9. **Li Z.** 2012. Regulation of the cell division cycle in *Trypanosoma brucei*. Eukaryot Cell **11:**1180–1190. http://dx.doi.org/10.1128/EC.00145-12.
10. **Robinson DR, Sherwin T, Ploubidou A, Byard EH, Gull K.** 1995. Microtubule polarity and dynamics in the control of organelle positioning, segregation, and cytokinesis in the trypanosome cell cycle. J Cell Biol **128:**1163–1172. http://dx.doi.org/10.1083/jcb.128.6.1163.
11. **Sherwin T, Gull K.** 1989. The cell division cycle of *Trypanosoma brucei brucei*: timing of event markers and cytoskeletal modulations. Philos Trans R Soc Lond B Biol Sci **323:**573–588. http://dx.doi.org/10.1098/rstb.1989.0037.
12. **Lacomble S, Vaughan S, Gadelha C, Morphew MK, Shaw MK, McIntosh JR, Gull K.** 2010. Basal body movements orchestrate membrane organelle division and cell morphogenesis in Trypanosoma brucei. J Cell Sci **123:**2884–2891. http://dx.doi.org/10.1242/jcs.074161.
13. **Woodward R, Gull K.** 1990. Timing of nuclear and kinetoplast DNA replication and early morphological events in the cell cycle of *Trypanosoma brucei*. J Cell Sci **95:**49–57.
14. **Gluenz E, Povelones ML, Englund PT, Gull K.** 2011. The kinetoplast duplication cycle in *Trypanosoma brucei* is orchestrated by cytoskeleton-mediated cell morphogenesis. Mol Cell Biol **31:**1012–1021. http://dx.doi.org/10.1128/MCB.01176-10.
15. **Ogbadoyi E, Ersfeld K, Robinson D, Sherwin T, Gull K.** 2000. Architecture of the Trypanosoma brucei nucleus during interphase and mitosis. Chromosoma **108:**501–513. http://dx.doi.org/10.1007/s004120050402.
16. **Robinson DR, Gull K.** 1991. Basal body movements as a mechanism for mitochondrial genome segregation in the trypanosome cell cycle. Nature **352:**731–733. http://dx.doi.org/10.1038/352731a0.
17. **Kohl L, Robinson D, Bastin P.** 2003. Novel roles for the flagellum in cell morphogenesis and cytokinesis of trypanosomes. EMBO J **22:**5336–5346. http://dx.doi.org/10.1093/emboj/cdg518.
18. **Vaughan S, Gull K.** 2008. The structural mechanics of cell division in Trypanosoma brucei. Biochem Soc Trans **36:**421–424. http://dx.doi.org/10.1042/BST0360421.
19. **Vaughan S, Kohl L, Ngai I, Wheeler RJ, Gull K.** 2008. A repetitive protein essential for the flagellum attachment zone filament structure and function in *Trypanosoma brucei*. Protist **159:**127–136. http://dx.doi.org/10.1016/j.protis.2007.08.005.
20. **Funato K, Vallée B, Riezman H.** 2002. Biosynthesis and trafficking of sphingolipids in the yeast *Saccharomyces cerevisiae*. Biochemistry **41:**15105–15114. http://dx.doi.org/10.1021/bi026616d.
21. **Ikonen E.** 2001. Roles of lipid rafts in membrane transport. Curr Opin Cell Biol **13:**470–477. http://dx.doi.org/10.1016/S0955-0674(00)00238-6.

22. **Hannun YA, Obeid LM**. 2011. Many ceramides. J Biol Chem **286:** 27855–27862. http://dx.doi.org/10.1074/jbc.R111.254359.
23. **Meivar-Levy I, Sabanay H, Bershadsky AD, Futerman AH**. 1997. The role of sphingolipids in the maintenance of fibroblast morphology. The inhibition of protrusional activity, cell spreading, and cytokinesis induced by fumonisin B1 can be reversed by ganglioside GM3. J Biol Chem **272:** 1558–1564. http://dx.doi.org/10.1074/jbc.272.3.1558.
24. **Merrill AH, Jr.** 2011. Sphingolipid and glycosphingolipid metabolic pathways in the era of sphingolipidomics. Chem Rev **111:**6387–6422. http://dx.doi.org/10.1021/cr2002917.
25. **Maceyka M, Payne SG, Milstien S, Spiegel S**. 2002. Sphingosine kinase, sphingosine-1-phosphate, and apoptosis. Biochim Biophys Acta **1585:** 193–201. http://dx.doi.org/10.1016/S1388-1981(02)00341-4.
26. **Gómez-Muñoz A**. 2006. Ceramide 1-phosphate/ceramide, a switch between life and death. Biochim Biophys Acta **1758:**2049–2056. http://dx.doi.org/10.1016/j.bbamem.2006.05.011.
27. **Zhang O, Hsu FF, Xu W, Pawlowic M, Zhang K**. 2013. Sphingosine kinase A is a pleiotropic and essential enzyme for Leishmania survival and virulence. Mol Microbiol **90:**489–501. http://dx.doi.org/10.1111/mmi.12378.
28. **Fridberg A, Olson CL, Nakayasu ES, Tyler KM, Almeida IC, Engman DM**. 2008. Sphingolipid synthesis is necessary for kinetoplast segregation and cytokinesis in *Trypanosoma brucei*. J Cell Sci **121:**522–535. http://dx.doi.org/10.1242/jcs.016741.
29. **Jensen BC, Sivam D, Kifer CT, Myler PJ, Parsons M**. 2009. Widespread variation in transcript abundance within and across developmental stages of Trypanosoma brucei. BMC Genomics **10:**482. http://dx.doi.org/10.1186/1471-2164-10-482.
30. **Siegel TN, Hekstra DR, Wang X, Dewell S, Cross GA**. 2010. Genome-wide analysis of mRNA abundance in two life-cycle stages of *Trypanosoma brucei* and identification of splicing and polyadenylation sites. Nucleic Acids Res **38:**4946–4957. http://dx.doi.org/10.1093/nar/gkq237.
31. **Lanterman MM, Saba JD**. 1998. Characterization of sphingosine kinase (SK) activity in *Saccharomyces cerevisiae* and isolation of SK-deficient mutants. Biochem J **332:**525–531. http://dx.doi.org/10.1042/bj3320525.
32. **Alsford S, Turner DJ, Obado SO, Sanchez-Flores A, Glover L, Berriman M, Hertz-Fowler C, Horn D**. 2011. High-throughput phenotyping using parallel sequencing of RNA interference targets in the African trypanosome. Genome Res **21:**915–924. http://dx.doi.org/10.1101/gr.115089.110.
33. **Hannun YA, Obeid LM**. 2008. Principles of bioactive lipid signalling: lessons from sphingolipids. Nat Rev Mol Cell Biol **9:**139–150. http://dx.doi.org/10.1038/nrm2329.
34. **Kilmartin JV, Wright B, Milstein C**. 1982. Rat monoclonal antitubulin antibodies derived by using a new nonsecreting rat cell line. J Cell Biol **93:**576–582. http://dx.doi.org/10.1083/jcb.93.3.576.
35. **Langousis G, Hill KL**. 2014. Motility and more: the flagellum of *Trypanosoma brucei*. Nat Rev Microbiol **12:**505–518. http://dx.doi.org/10.1038/nrmicro3274.
36. **Edsall LC, Van Brocklyn JR, Cuvillier O, Kleuser B, Spiegel S**. 1998. N,N-dimethylsphingosine is a potent competitive inhibitor of sphingosine kinase but not of protein kinase C: modulation of cellular levels of sphingosine 1-phosphate and ceramide. Biochemistry **37:**12892–12898. http://dx.doi.org/10.1021/bi980744d.
37. **Olivera A, Kohama T, Tu Z, Milstien S, Spiegel S**. 1998. Purification and characterization of rat kidney sphingosine kinase. J Biol Chem **273:** 12576–12583. http://dx.doi.org/10.1074/jbc.273.20.12576.
38. **Hendriks EF, Robinson DR, Hinkins M, Matthews KR**. 2001. A novel CCCH protein which modulates differentiation of *Trypanosoma brucei* to its procyclic form. EMBO J **20:**6700–6711. http://dx.doi.org/10.1093/emboj/20.23.6700.
39. **Hammarton TC, Engstler M, Mottram JC**. 2004. The *Trypanosoma brucei* cyclin, CYC2, is required for cell cycle progression through G1 phase and for maintenance of procyclic form cell morphology. J Biol Chem **279:**24757–24764. http://dx.doi.org/10.1074/jbc.M401276200.
40. **Patti GJ, Yanes O, Shriver LP, Courade JP, Tautenhahn R, Manchester M, Siuzdak G**. 2012. Metabolomics implicates altered sphingolipids in chronic pain of neuropathic origin. Nat Chem Biol **8:**232–234. http://dx.doi.org/10.1038/nchembio.767.
41. **Nagiec MM, Skrzypek M, Nagiec EE, Lester RL, Dickson RC**. 1998. The LCB4 (YOR171c) and LCB5 (YLR260w) genes of Saccharomyces encode sphingoid long chain base kinases. J Biol Chem **273:**19437–19442. http://dx.doi.org/10.1074/jbc.273.31.19437.
42. **Allende ML, Sasaki T, Kawai H, Olivera A, Mi Y, van Echten-Deckert G, Hajdu R, Rosenbach M, Keohane CA, Mandala S, Spiegel S, Proia RL**. 2004. Mice deficient in sphingosine kinase 1 are rendered lymphopenic by FTY720. J Biol Chem **279:**52487–52492. http://dx.doi.org/10.1074/jbc.M406512200.
43. **Mizugishi K, Yamashita T, Olivera A, Miller GF, Spiegel S, Proia RL**. 2005. Essential role for sphingosine kinases in neural and vascular development. Mol Cell Biol **25:**11113–11121. http://dx.doi.org/10.1128/MCB.25.24.11113-11121.2005.
44. **Shen H, Giordano F, Wu Y, Chan J, Zhu C, Milosevic I, Wu X, Yao K, Chen B, Baumgart T, Sieburth D, De Camilli P**. 2014. Coupling between endocytosis and sphingosine kinase 1 recruitment. Nat Cell Biol **16:** 652–662. http://dx.doi.org/10.1038/ncb2987.
45. **Wirtz E, Leal S, Ochatt C, Cross GA**. 1999. A tightly regulated inducible expression system for conditional gene knockouts and dominant-negative genetics in *Trypanosoma brucei*. Mol Biochem Parasitol **99:**89–101. http://dx.doi.org/10.1016/S0166-6851(99)00002-X.
46. **Doyle JJ, Hirumi H, Hirumi K, Lupton EN, Cross GA**. 1980. Antigenic variation in clones of animal-infective *Trypanosoma brucei* derived and maintained in vitro. Parasitology **80:**359–369. http://dx.doi.org/10.1017/S0031182000000810.
47. **Brun R, Schönenberger**. 1979. Cultivation and in vitro cloning or procyclic culture forms of *Trypanosoma brucei* in a semi-defined medium. Short communication. Acta Trop **36:**289–292.
48. **Sundström C, Nilsson K**. 1976. Establishment and characterization of a human histiocytic lymphoma cell line (U-937). Int J Cancer **17:**565–577. http://dx.doi.org/10.1002/ijc.2910170504.
49. **Redmond S, Vadivelu J, Field MC**. 2003. RNAit: an automated web-based tool for the selection of RNAi targets in *Trypanosoma brucei*. Mol Biochem Parasitol **128:**115–118. http://dx.doi.org/10.1016/S0166-6851(03)00045-8.
50. **Wang Z, Morris JC, Drew ME, Englund PT**. 2000. Inhibition of *Trypanosoma brucei* gene expression by RNA interference using an integratable vector with opposing T7 promoters. J Biol Chem **275:**40174–40179. http://dx.doi.org/10.1074/jbc.M008405200.
51. **Mutomba MC, To WY, Hyun WC, Wang CC**. 1997. Inhibition of proteasome activity blocks cell cycle progression at specific phase boundaries in African trypanosomes. Mol Biochem Parasitol **90:**491–504. http://dx.doi.org/10.1016/S0166-6851(97)00197-7.